Optik - International Journal for Light and Electron Optics 172 (2018) 980–987

Contents lists available at ScienceDirect

Optik

journal homepage: www.elsevier.com/locate/ijleo

Original research article

Polarization radiometric calibration method for multichannel polarization camera

Yi Li[a,b], Haiyang Zhang[a,b], Wei Liu[a,*], Changxiang Yan[a]

[a] Changchun Institute of Optics, Fine Mechanics and Physics, Chinese Academy of Science, Changchun 130033, China
[b] University of Chinese Academy of Science, Beijing 100049, China

ARTICLE INFO

Keywords:
Polarization radiometric imaging
Multichannel polarization camera
Calibration
Remote sensing and sensors

ABSTRACT

In the field of space remote sensing, multichannel polarization camera, which records the radiance of the transmitted light at several specific angles simultaneously, plays a significant role. However, the nonuniform response among different channels will lead to measurement error. Since the polarization parameters of polarization elements are ignored in traditional radiometric calibration, so for multichannel polarization camera, the traditional calibration is not suitable. To cope with this issue, a polarimetric calibration will be introduced below. In this paper a polarization radiometric calibration method for a multichannel polarization camera is presented. A polarization radiometric calibration model is proposed in this paper to analytically describe the responses of digital number of the detector to the radiance of the incident light and the polarization parameters of polarization elements. Through a verification experiment, the polarization parameters and polarization radiometric calibration coefficients of a simulated polarization camera were obtained rapidly. Results of the experiment indicates that the accuracy of the final calibration is 0.8% at 670 nm. The proposed polarization radiometric calibration method can be used in the calibration of the multichannel polarization camera and satisfy the requirements of the existing polarization remote sensing detection.

1. Introduction

The polarization property of light can convey a wealth of information [1,2]. Through analyzing the state of polarization of reflected light by a target, we can obtain valuable information about the surface features and material composition. This makes polarization detection a powerful tool in the fields of agriculture, military affairs [3,4], and study of meteorological environment [5]. Some space-based polarization remote sensing devices are well known such as the Polarization and Directionality of the Earth's Reflectance (POLDER) [6], Earth Observing Scanning Polarimeter (EOSP) [7], and Cloud and Aerosol Polarimetric Imager (CAPI) [8]. At present, most of these instruments are first-generation polarization detection systems include the division-of-time, division-of-amplitude, division-of-aperture, and division-of-focal plane [9] types of systems. Compared with the above methods, multichannel division-of-amplitude polarization detection is a suitable method for polarization imaging remote sensing, as done in CAPI. Despite its higher cost, it is of plenty advantages such as high maturity and stability and instantaneous plane array imaging.

In multichannel cameras, nonuniform correction among channels is a common problem, especially with multichannel polarization cameras, for which the detection results are calculated based on the radiance received by each channel [10]. For conventional multichannel cameras, the correction is done via radiometric calibration for each channel. However, the polarization camera with

* Corresponding author.
E-mail address: liuwei_ciomp@163.com (W. Liu).

https://doi.org/10.1016/j.ijleo.2018.07.083
Received 21 May 2018; Accepted 22 July 2018

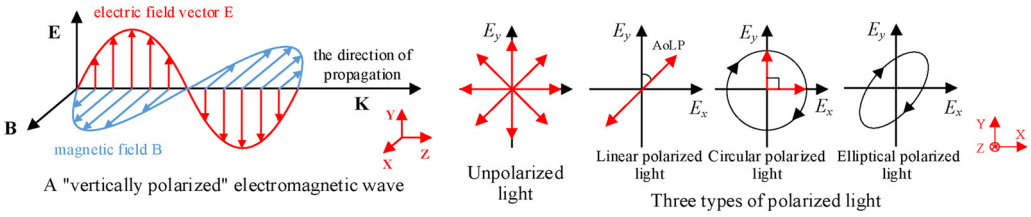

Fig. 1. Electromagnetic waves and the state of polarization.

radiometric calibration is of more complexity. Polarization camera contains some polarization elements [11] whose polarization parameters should be included in the calibration model. The traditional radiometric calibration model is not feasible for the polarization camera because this model assumes that the polarization effects of each element can be ignored.

In this paper, a new calibration model called polarization radiometric calibration model is proposed to correct the nonuniform response among channels. This model contains the polarization parameters of each element. The measurement of the polarization parameters is the key point for ensuring calibration accuracy. There is a rotating linear polarizer in measurement system, which is easier to operate and control, to obtain the parameters. An approximate cosine curve is obtained by rotating the linear polarizer continuously. With the application of a novel model established in this paper, the polarization parameters were calculated precisely. The experimental results show that the proposed model is sufficient for the nonuniform correction of the multichannel polarization camera.

This paper is organized as follows. In Section 2, the basic principle of a multichannel polarization camera [8] was introduced and the traditional radiometric calibration process for the camera was described. In Section 3, a new polarization radiometric calibration model was established for the system by analyzing the process of polarized radiation transmission, and a high-precision measurement method was proposed to obtain the polarization parameters. In Section 4, a verification experiment conducted to verify the accuracy of the proposed polarization radiometric calibration method was described. In Section 5, we summarize and conclude the paper.

2. Traditional radiometric calibration for the multichannel polarization camera

2.1. The multichannel polarization camera

The state of polarization contains a great deal of information [12]. As is shown in Fig. 1, the state of polarization consists of unpolarized light, polarized light (linear polarized, circular polarized, and elliptical polarized), and partially polarized light [13] (a combination of unpolarized and polarized light).

In the field of remote sensing, the state of polarization of reflected light is always considered as partially linear polarized light, and the circular polarization component can be ignored. Partially linear polarized light is shown in Fig. 2. The degree of linear polarization (*DoLP*) and the angle of linear polarization (*AoLP*) were often used to describe the state of polarization of the partially linear polarized light [14], where *DoLP* represents the proportion of the linear polarized light among all the state of polarization of light (unpolarized and linear polarized), and *AoLP* represents the oscillation direction of the linear polarized light.

To measure the state of polarization of the partially linear polarized light, a simple method employing a rotating linear polarizer (herein, called the analyzer) was adopted [15]. The schematic of the measurement method for the state of polarization of partially linear polarized light is shown in Fig. 3. The analyzer is placed perpendicular to the incident light, and rotated from 0° to 180°. By recording the radiance of the transmitted light at three specific angles (0°, 60°, and 120°), the *DoLP* and *AoLP* were obtained by using Eq. (1). This method is called division-of-time method, implying that the measurement cannot be completed instantaneously.

$$DoLP = \sqrt{\frac{Q^2+U^2}{I^2}},\ AoLP = \frac{1}{2}a\tan\left(\frac{U}{Q}\right),$$
$$\begin{cases} I = \frac{2}{3}(I_{0°} + I_{60°} + I_{120°}) \\ Q = \frac{2}{3}(2I_{0°} - I_{60°} - I_{120°}). \\ U = \frac{2}{\sqrt{3}}(I_{60°} - I_{120°}) \end{cases} \tag{1}$$

The multichannel polarization camera uses an improvement of the above mentioned method. To complete the measurement

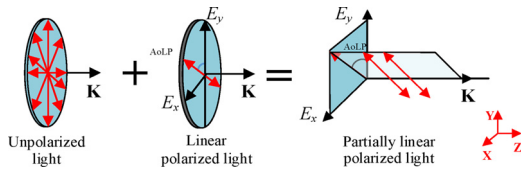

Fig. 2. Partially linear polarized light.

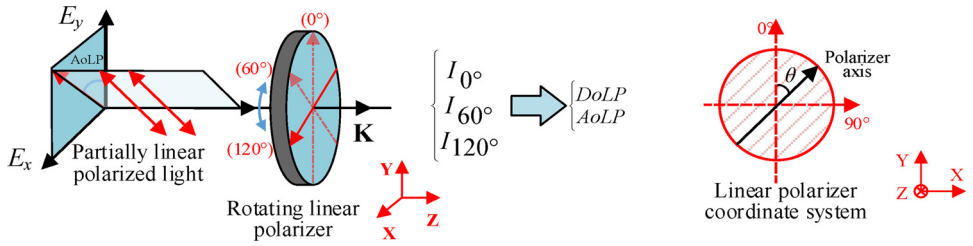

Fig. 3. Measurement method for the state of polarization of partially linear polarized light.

simultaneously, the rotating analyzer is placed with three fixed analyzers with polarization axis angles of 0°, 60°, and 120°. This would disperse the incident light into three beams and this method is called the division-of-amplitude method.

The schematic of the multichannel polarization camera is shown in Fig. 4. The structure of the camera is similar to that of an ordinary imaging camera. The image of the target is collected by the optical lens, and received by the detector. However, the incident light is dispersed into three beams by the beam splitter behind the optical lens in the multichannel polarization camera. These beams are received by three distinct detectors placed after the three linear polarizers with each polarization axis angles at 0°, 60°, and 120°.

By using the polarization camera, the light intensity of the three analyzer channels ($I_{0°}$, $I_{60°}$, and $I_{120°}$) could be recorded simultaneously. Thus, the *DoLP* and *AoLP* were obtained using Eq. (1) through only one measurement, which could be used for the inversion of target characteristics [16].

Generally, the multichannel polarization camera is, in essence, a multichannel camera. The main difference between the two is that in the polarization camera, three linear polarizers are placed between the beam splitter and the detectors, and the detection result is more sensitive to the nonuniform response among the channels.

2.2. The traditional radiometric calibration

The nonuniform response among the channels in the multichannel camera can be corrected by radiometric calibration. Since detectors only respond to light intensity, traditional radiometric calibration is based on the radiation transmission theory, and which ignores the polarization effects of the elements. The radiance of the incident light is reduced by the optical lens, the beam splitter, and the linear polarizers, whose transmittances are expressed as $\overline{T}_{opt}$, T_0, and $\overline{T}_x$, respectively. When the radiance of the incident light is I, the intensity of the light I_{out} received by each channel is $I_{out} = \overline{T}_{opt} \cdot T_0 \cdot \overline{T}_x \cdot I$.

According to the principle of radiometric calibration [10], the relationship between radiance at the entrance pupil and the *DN* response of the detector is

$$I = A(DN - C) + B. \tag{2}$$

where C is the dark current response, A and B are the absolute radiometric calibration coefficients, namely, the linear response coefficient and the constant response coefficient. The physical significance of the coefficients is that they convey information on the total transmittance of the camera, the responsivity of the detector, and so on.

The schematic of the traditional radiometric calibration for each analyzer channel is shown in Fig. 5. The absolute radiometric calibration coefficients A and B can be obtained by changing the radiance of the incident light I several times. By applying radiometric calibration to each channel, the nonuniform response among the channels can be corrected.

However, the detection result of the polarization camera is still inaccurate despite the traditional radiometric calibration through an integrating sphere. The main reason is that the polarization effects of some elements (e.g. the linear polarizer and the optical lens) are ignored in the procedure. When considering the polarization effects of these elements, it should be noted that their effective

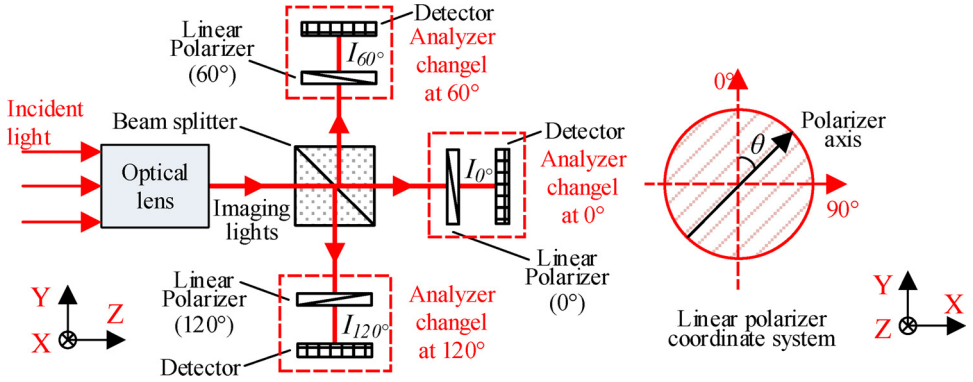

Fig. 4. Schematic of the multichannel polarization camera.

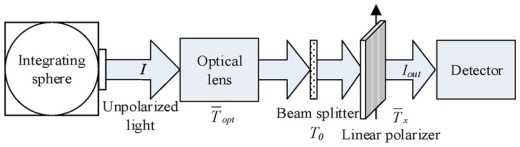

Fig. 5. Traditional radiometric calibration for each analyzer channel.

transmittance is related to the state of polarization of the incident light, and they should be described by the maximum transmittance and extra-polarization parameters.

Therefore, traditional radiometric calibration cannot be used directly for the polarization camera because the polarization parameters of polarization elements are not considered in this calibration. The calibration method should be modified for the multichannel polarization camera based on polarization optics theory.

3. The polarization radiometric calibration model of the multichannel polarization camera

3.1. Polarization radiometric calibration model based on polarization optics theory

For most optical lenses, some polarization effects, which change with the field of view, are inevitable. These effects result from the optical structure and coating [14]. The influence of these effects can be ignored on the ordinary camera. However, it needs to be considered in the case of the polarization camera because it leads to extra errors in polarization detection. For a refractive optical system, according to the polarization optics theory [17], the polarization effects mainly include diattenuatation and phase retardance. Noteworthy is that we do not consider the phase retardance in this paper. Because the phase retardance of the optical systems we studied is 3.5×10^{-2}rad calculated by the polarization tracing [18]. The low phase retardance can be ignored during the process of the polarization radiometric calibration. The diattenuatation can be represented by the angle of polarization θ_1 and the degree of polarization $\varepsilon_1 = (T_s - T_p)/(T_s + T_p)$, where T_s and T_p represent the transmittance in the two orthogonal directions [13]. If the circularly polarized component is ignored, the Mueller matrices [14] for the refractive optical system can be given by

$$\mathbf{M_T} = \mathbf{R}(-\theta_1)\cdot\frac{1}{2}\begin{bmatrix} T_S + T_P & T_S - T_P & 0 \\ T_S - T_P & T_S + T_P & 0 \\ 0 & 0 & 2\sqrt{T_S T_P} \end{bmatrix}\cdot\mathbf{R}(\theta_1), \tag{3}$$

where $\mathbf{R}(-\theta_1)$, $\mathbf{R}(\theta_1)$ are the rotation matrices [17]. By using ε_1 to replace T_s and T_p, Eq. (3) can be rewritten as

$$\mathbf{M_T} = \mathbf{R}(-\theta_1)\cdot\frac{T_S + T_P}{2}\begin{bmatrix} 1 & \varepsilon_1 & 0 \\ \varepsilon_1 & 1 & 0 \\ 0 & 0 & \sqrt{1-\varepsilon_1^2} \end{bmatrix}\cdot\mathbf{R}(\theta_1). \tag{4}$$

Then the Mueller matrices of the front optical lens are obtained as

$$\mathbf{M_T}(\theta_1, \varepsilon_1, \omega, \varphi) = \frac{T_S + T_P}{2}\begin{bmatrix} 1 & \varepsilon_1\cos 2\theta_1 & \varepsilon_1 \sin 2\theta_1 \\ \varepsilon_1\cos 2\theta_1 & \cos^2 2\theta_1 + \sqrt{1-\varepsilon_1^2}\sin^2 2\theta_1 & (1-\sqrt{1-\varepsilon_1^2})\cos 2\theta_1 \sin 2\theta_1 \\ \varepsilon_1 \sin 2\theta_1 & (1-\sqrt{1-\varepsilon_1^2})\cos 2\theta_1 \sin 2\theta_1 & \sin^2 2\theta_1 + \sqrt{1-\varepsilon_1^2}\cos^2 2\theta_1 \end{bmatrix}, \tag{5}$$

where (ω, φ) represents the different fields of view within each channel. Because the degree of polarization ε_1 and the angle of polarization θ_1 corresponding to different fields of view are different, Mueller matrices $\mathbf{M_T}(\theta_1, \varepsilon_1, \omega, \varphi)$ are written as shown in Eq. (5) for each viewing angle.

For the linear polarizer (herein, called the analyzer) of the polarization camera, t_x^2 and t_y^2 are used to describe the maximum and minimum transmittance in the two orthogonal directions [17]. Meanwhile, $\varepsilon^2 = t_y^2/t_x^2$ describes the extinction ratio of the analyzer, and θ describes the transmission axis angle (0°, 60°, and 120°) of the analyzer in different channels. Thus, the Mueller matrix of the analyzer is expressed as

$$\mathbf{M_p}(\varepsilon^2, \theta) = \frac{t_x^2}{2}\begin{bmatrix} 1+\varepsilon^2 & (1-\varepsilon^2)\cos 2\theta & (1-\varepsilon^2)sin2\theta \\ (1-\varepsilon^2)\cos 2\theta & (1-\varepsilon^2)\cos^2 2\theta + 2\varepsilon sin^2 2\theta & (1-\varepsilon)^2\cos 2\theta sin2\theta \\ (1-\varepsilon^2)sin2\theta & (1-\varepsilon)^2\cos 2\theta sin2\theta & (1-\varepsilon)^2 sin^2 2\theta + 2\varepsilon \end{bmatrix}. \tag{6}$$

When the polarization camera is used for polarization radiometric calibration, the light from an integrating sphere light source can be assumed to be unpolarized. We assume the incident radiance as I, and its Stokes vector as $\boldsymbol{S}_{\mathbf{in}} = [I \quad 0 \quad 0]^T$. According to the theory of polarization radiation transmission, the Stokes vector at the detector of each channel is calculated as $\mathbf{S_{out}} = T_0\cdot\mathbf{M_P}(\varepsilon^2, \theta)\cdot\mathbf{M_T}(\theta_1, \varepsilon_1, \omega, \varphi)\cdot\mathbf{S_{in}}$. The polarization transmission diagram is shown in Fig. 6. Here, the polarization effect of the beam splitter is included in the effect of the optical lens, and its transmittance is T_0.

Since the transmittance of the beam splitter of each analyzer channel is different, we can use $T_{sys} = T_0 t_x^2 (T_s + T_p)$ to describe the system transmission factor of each analyzer channel. Then, the Stokes vector can be rewritten as

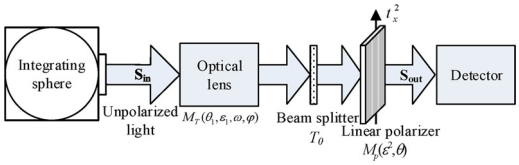

Fig. 6. Polarization radiation transmission of each analyzer channel.

$$\begin{bmatrix} I_{out} \\ Q_{out} \\ U_{out} \end{bmatrix} = \frac{T_{sys}}{4} \begin{bmatrix} 1+\varepsilon^2 & (1-\varepsilon^2)cos2\theta & (1-\varepsilon^2)sin2\theta \\ (1-\varepsilon^2)cos2\theta & (1-\varepsilon^2)cos^2 2\theta + 2\varepsilon sin^2 2\theta & (1-\varepsilon)^2 cos2\theta sin2\theta \\ (1-\varepsilon^2)sin2\theta & (1-\varepsilon)^2 cos2\theta sin2\theta & (1-\varepsilon)^2 sin^2 2\theta + 2\varepsilon \end{bmatrix} \cdot \begin{bmatrix} 1 & \varepsilon_1 cos2\theta_1 & \varepsilon_1 sin2\theta_1 \\ \varepsilon_1 cos2\theta_1 & cos^2 2\theta_1 + \sqrt{1-\varepsilon_1^2} sin^2 2\theta_1 & (1-\sqrt{1-\varepsilon_1^2}) cos2\theta_1 sin2\theta_1 \\ \varepsilon_1 sin2\theta_1 & (1-\sqrt{1-\varepsilon_1^2}) cos2\theta_1 sin2\theta_1 & sin^2 2\theta_1 + \sqrt{1-\varepsilon_1^2} cos^2 2\theta_1 \end{bmatrix} \begin{bmatrix} I \\ 0 \\ 0 \end{bmatrix}. \tag{7}$$

The light radiance received by the detector is

$$I_{out} = \frac{T_{sys} I}{4}[(1+\varepsilon^2) + \varepsilon_1(1-\varepsilon^2)cos2(\theta-\theta_1)]. \tag{8}$$

Substituting Eqs. (8) into (2) yields the polarization radiometric calibration model of the polarization camera,

$$\frac{I}{4}[(1+\varepsilon^2) + \varepsilon_1(1-\varepsilon^2)\cos 2(\theta-\theta_1)] = A(DN-C) + B. \tag{9}$$

The dark current response C in Eq. (9) can be obtained by covering the lens. Here, A and B represent the absolute polarization radiometric calibration coefficients, and they contain information on the system transmission factor T_{sys}, responsivity of the detector, and so on. The polarization parameters ε^2, ε_1, and θ_1 are the system parameters that have to be measured. When the polarization parameters are known, the incident light radiance I is changed several times. Then, the linear relationship between the incident light radiance I and the DN response of the detector can be obtained. By a linear least-squares fit, the absolute polarization radiometric calibration coefficients A and B can be obtained.

From the calibration model we can see that the factors influencing the polarization radiometric calibration precision are as follows: the uniformity and stability of the integrating sphere light source, the measurement precision of light radiance, dark current response, and the polarization parameters ε^2, ε_1, and θ_1. Considering the performance of the integrating sphere light source is excellent [19], and the light radiance measurement by ASD spectrometer is accurate [20], and the dark current of detector is very low, the factors that restrict the precision of polarization radiometric calibration were the measurement accuracy of the polarization parameters.

3.2. Measurement for polarization parameters

When the incident light is linear polarized light with continuously changing orientation (intensity constant), the information of polarization parameters is hidden in the changing of received light intensity. This situation is shown schematically in Fig. 7.

Here, the radiance of the polarized light is considered as I_0, and the orientation is considered as θ_0. Then the corresponding Stokes vector is $\mathbf{S'_{in}} = I_0[1\ \cos 2\theta_0\ \sin 2\theta_0]^T$. According to the polarization radiation transmission theory, the Stokes vector of the light reaching the detector is

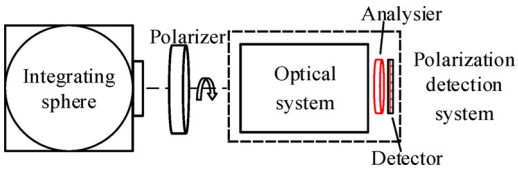

Fig. 7. Diagram of the calibration system.

$$\begin{bmatrix} I'_{out} \\ Q'_{out} \\ U'_{out} \end{bmatrix} = \frac{T_{sys}I_0}{4}\begin{bmatrix} 1+\varepsilon^2 & (1-\varepsilon^2)cos2\theta & (1-\varepsilon^2)sin2\theta \\ (1-\varepsilon^2)cos2\theta & (1-\varepsilon^2)cos^2 2\theta + 2\varepsilon sin^2 2\theta & (1-\varepsilon)^2 cos2\theta sin2\theta \\ (1-\varepsilon^2)sin2\theta & (1-\varepsilon)^2 cos2\theta sin2\theta & (1-\varepsilon)^2 sin^2 2\theta + 2\varepsilon \end{bmatrix} \cdot \begin{bmatrix} 1 & \varepsilon_1 cos2\theta_1 & \varepsilon_1 sin2\theta_1 \\ \varepsilon_1 cos2\theta_1 & cos^2 2\theta_1 + \sqrt{1-\varepsilon_1^2} sin^2 2\theta_1 & (1-\sqrt{1-\varepsilon_1^2})cos2\theta_1 sin2\theta_1 \\ \varepsilon_1 sin2\theta_1 & (1-\sqrt{1-\varepsilon_1^2})cos2\theta_1 sin2\theta_1 & sin^2 2\theta_1 + \sqrt{1-\varepsilon_1^2} cos^2 2\theta_1 \end{bmatrix} \begin{bmatrix} 1 \\ \cos 2\theta_0 \\ \sin 2\theta_0 \end{bmatrix}. \tag{10}$$

The light intensity I'_{out} that changes with the orientation θ_0 is

$$\begin{cases} I'_{out}(\theta_0, \theta) = \frac{T_{sys}I_0}{8}\{1 + \varepsilon^2 + \varepsilon_1(1-\varepsilon^2)\cos 2(\theta - \theta_1) + \cos 2\theta_0 \Gamma_1 + \sin 2\theta_0 \Gamma_2\} \\ \Gamma_1 = \varepsilon_1 \cos 2\theta_1 (1+\varepsilon^2) + \cos 2\theta(\cos^2 2\theta_1 + \sqrt{1-\varepsilon_1^2}\sin^2 2\theta_1)(1-\varepsilon^2) + \sin 2\theta \cos 2\theta_1 \sin 2\theta_1 (1-\sqrt{1-\varepsilon_1^2})(1-\varepsilon^2) \\ \Gamma_2 = \varepsilon_1 \sin 2\theta_1 (1+\varepsilon^2) + \sin 2\theta(\sin^2 2\theta_1 + \sqrt{1-\varepsilon_1^2}\cos^2 2\theta_1)(1-\varepsilon^2) + \cos 2\theta \cos 2\theta_1 \sin 2\theta_1 (1-\sqrt{1-\varepsilon_1^2})(1-\varepsilon^2) \end{cases} \tag{11}$$

For each analyzer channel, the *DN* response of the detector after dark current correction is approximately proportional to the received light intensity. For each field of view, the relationship between *DN* response and θ_0 changes as Eq. (11). By using the least-squares fitting to the *DN* response data, the polarization parameters ε^2, ε_1, and θ_1 corresponding to each viewing angle can be obtained exactly.

The polarization radiometric calibration of the multichannel polarization camera is presented in the above analysis. For the apparatus used, such as the integrating sphere, linear polarizer (polarizer), and ASD spectrometer, are high-precision systems, the main influence factor is the fitting accuracy.

4. Experimental results

In the verifying experiment, a refractive optical system is used as the front optical lens of the polarization camera. A rotating linear polarizer (analyzer) and an ASD detector (single viewing angle) [20] are placed on the back focal plane. Thus, a polarization detection system is simulated. The linear polarized light necessary for measuring the polarization parameters is obtained through an integrating sphere light source and a rotating linear polarizer (polarizer) [21]. Because of the restrictions in viewing angle imposed by the detector, polarization radiometric calibration method is performed only for a certain field of view.

4.1. Polarization parameters measurement

Firstly, the optical axis of the integrating sphere, linear polarizer (polarizer), the refractive optical system, the linear polarizer (analyzer), and the detector are adjusted to be coaxial. Secondly, the ASD detector is placed on the focal plane of the refractive optical system. Thirdly, the linear polarizer (polarizer) is rotated from 0° to 340°, and the rotation was precisely controlled by a Newport rotation stage. The *DN* response of the detector was simultaneously recorded. The measurement system is shown in Fig. 8.

The experimental data (after dark current correction) and the fitting curve obtained through Eq. (11) are shown in Fig. 9. The fitting results show that the polarization parameters (670 nm) of the simulated polarization camera are obtained: extinction ratio $\varepsilon^2 = 1/400$, the degree of polarization $\varepsilon_1 = 5.61\%$, and the angle of polarization $\theta_1 = 92°$.

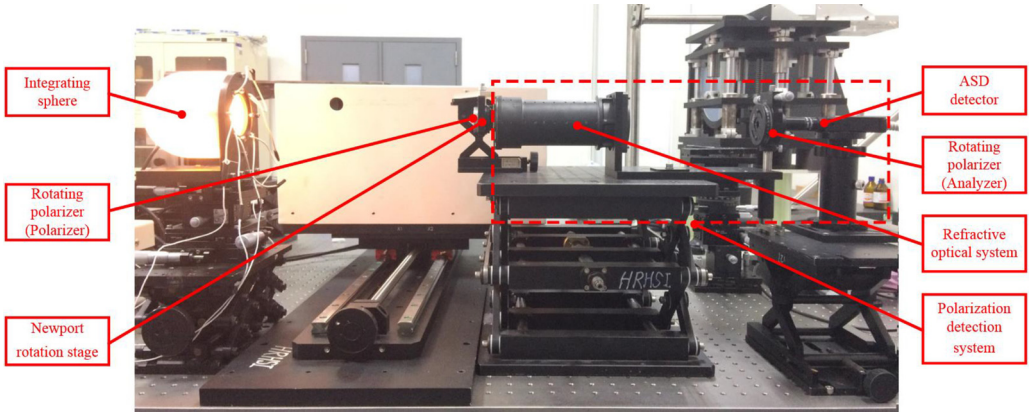

Fig. 8. Photograph of measurement system setup for polarization parameters.

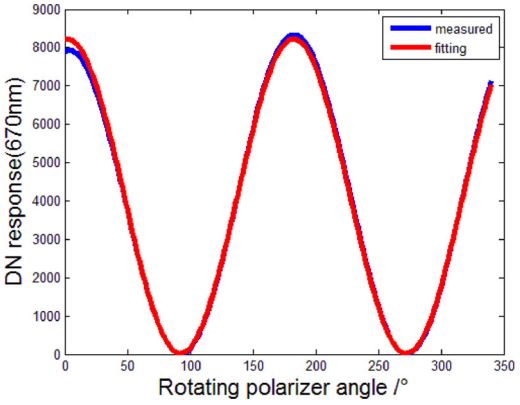

Fig. 9. Experimental data and the model fitting curve of the polarization parameters.

4.2. Absolute polarization radiometric calibration coefficients

The linear polarizer (polarizer) is taken off to enable unpolarized light to go through the simulated polarization camera. Then the radiance level of the integrating sphere is changed for several times. Simultaneously, the corresponding *DN* response and the light radiance at the entrance pupil of the camera were recorded. The calibration system is shown in Fig. 10.

The absolute polarization radiometric calibration coefficients could be fitted by the linear polarization radiometric calibration model. The fitting result is shown in Fig. 11. According to the fitting results, the absolute polarization radiometric calibration coefficients of the simulated polarization camera are as follows: $A = 6.7198*10^{-5}$W/(m^2*nm*sr), $B = -9.4*10^{-5}$ W/(m^2*nm*sr) (670 nm). The precision of polarization radiometric calibration could be verified via the calibrated system with the relative error shown in Fig. 11. We can conclude that the precision of the radiation calibration was 0.8% at 670 nm between the fitting results and the directly measured results.

5. Conclusions

In this paper, a complete framework of the radiometric calibration for the multichannel polarization camera is presented. Firstly, the basic structure of the multichannel polarization camera is introduced, and the necessity of radiometric calibration for the polarization camera is discussed. Secondly, the polarization effects of optical lens and linear polarizer (analyzer) are analyzed based on the polarization optics theory. The polarization radiation transmission model of the polarization camera is derived. A new radiometric calibration model of the polarization camera is established, including polarization parameters and absolute radiometric calibration coefficients. To obtain the polarization parameters, a new measurement method of high precision is proposed. Finally, the radiometric calibration for a simulated polarization camera is achieved successfully. The results show that, the final accuracy is 0.8%, which satisfies the requirements of current polarization remote sensing detection. In conclusion, this paper provides important bases for polarization detection and polarized characteristics inversion.

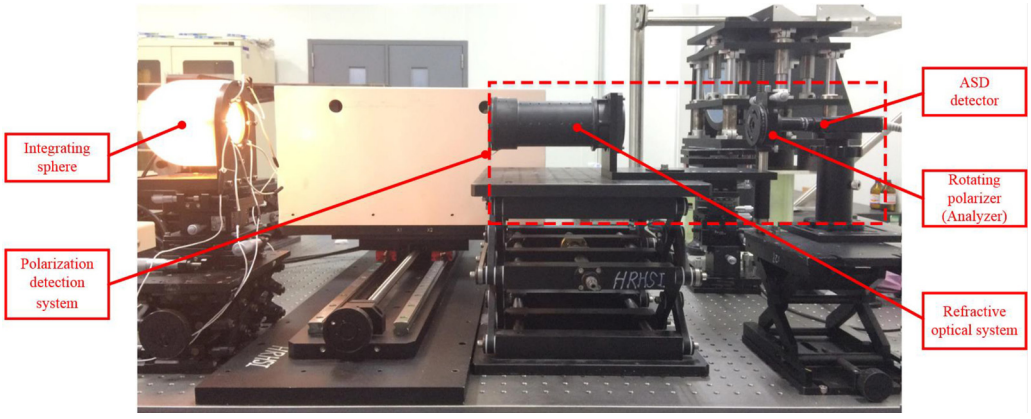

Fig. 10. Photograph of the setup for absolute polarization radiometric calibration.

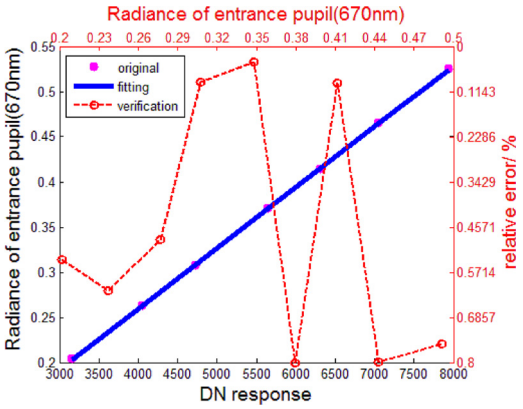

Fig. 11. Absolute polarization radiometric calibration curve and precision verification results.

Acknowledgements

This work was supported by the National Key Research and Development Program of China [grant number 2016YFF0103603] and National Natural Science Foundation of China [grant number 61505199]. The authors would like to thank the anonymous reviewers for their useful comments and critical remarks which helped to improve this paper.

References

[1] T. York, Bioinspired polarization imaging sensors: from circuits and optics to signal processing algorithms and biomedical applications, Proc. IEEE 102 (10) (2014) 1450–1469.
[2] S. Gao, V. Gruev, Bilinear and bicubic interpolation methods for division of focal plane polarimeters, Opt. Express 19 (27) (2011) 26161–26173.
[3] J.S. Tyo, D.L. Goldstein, D.B. Chenault, Joseph A. Shaw, Review of passive imaging polarimetry for remote sensing applications, Appl. Opt. 45 (22) (2006) 5453–5469.
[4] Y.H. Zhan, Q. Liu, D. Yang, et al., nversion of complex refractive index for rough-surface objects, Opt. Precis. Eng. 23 (8) (2015) 2178–2184.
[5] L.G. Tilstra, P. Stammes, Earth reflectance and polarization intercomparison between SCIAMACHY onboard Envisat and POLDER onboard ADEOS-2, J. Geophys. Res. 112 (2007) D11304.
[6] P.Y. Deschamps, F.M. Bron, M. Leroy, et al., The POLDER mission: instrument characteristics and scientific objectives, Proc. IEEE 32 (3) (1994) 598–615.
[7] L.D. Travis, Remote sensing of aerosols with the earth observing scanning polarimeter, Proc. SPIE. 1747 (1992) 154–164.
[8] J.Q. Zhang, C. Xue, Z.L. Gao, et al., Optical remote sensor for cloud and aerosol from space: past, present and future, Chin. Opt. 8 (5) (2015) 679–698.
[9] B.M. Ratliff, C.F. LaCasse, J.S. Tyo, Interpolation strategies for reducing IFOV artifacts in microgrid polarimeter imagery, Opt. Express 17 (11) (2009) 9112–9125.
[10] L.L. Zheng, Correction of non-uniformity response for multiple output TDI CCD imaging system, Infrared Laser Eng. 43 (S) (2014) 145–150.
[11] O. Morel, R. Seulin, D. Fofi, Handy method to calibrate division-of-amplitude polarimeters for the first three Stokes parameters, Opt. Express 24 (12) (2016) 13634–13646.
[12] J. Xu, W. Qian, Q. Chen, Calculation model of scattering depolarization for camouflaged target detection system, Optik 158 (2018) (2018) 341–348.
[13] S.X. Shi, X.E. Wang, J.S. Liu, Physical Optics and Applied Optics, Xidian University Publisher, 2008.
[14] R.A. Chipman, M. Bass (Ed.), Handbook of Optics, McGraw-Hill, 2009.
[15] Y.Q. Zhao, Q. Pan, Y.M. Cheng, Imaging Spectropolarimetric Remote Sensing and Application, National Defense Industry Press, Beijing, 2011, p. 43.
[16] B. Yang, C.X. Yan, J.Q. Zhang, H.Y. Zhang, Refractive index and surface roughness estimation using passive multispectral and multiangular polarimetric measurements, Opt. Commun. 381 (2016) 336–345.
[17] Y.B. Liao, Polarization Optics, Science Press, 2003 Chap. 2.
[18] D.M. Harrington, S.R. Sueoka, Polarization modeling and predictions for Daniel K. Inouye Solar Telescope part 1: telescope and example instrument configurations, J. Astron. Telesc. Instrum. Syst. 3 (1) (2017) 018002.
[19] L. Mikheenko, V. Borovytsky, Metrological advantages of the light source based on optically connected integrating spheres, Proc. SPIE. 8511 (2014) 851113.
[20] ASD, Field Spec 4 Standard-Res Spectroradiometer, http://www.asdi.com/products-and-services/fieldspec-spectroradiometers/fieldspec-4-standard-res.
[21] M.X. Song, B. Sun, X.B. Sun, et al., Polarization calibration of airborne multi-angle polarimetric radiometer, Opt. Precis. Eng. 20 (6) (2012) 1153–1158.